

1.1. ELEMENTARY MODES OF EXCITATION

13

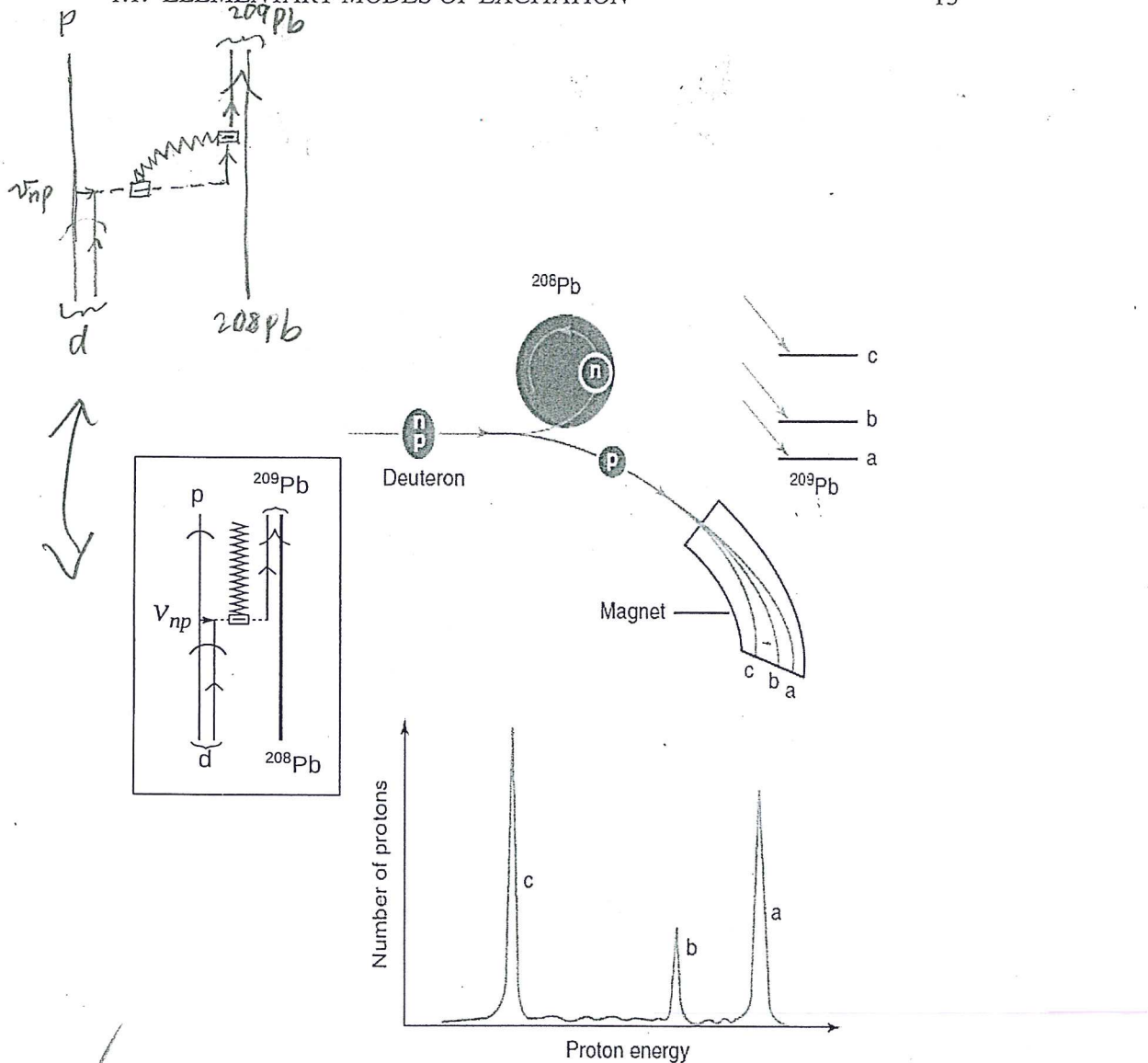


Figure 1.1.2: (Color online) Schematic representation of the one-nucleon transfer reaction $^{208}\text{Pb}(d, p)^{209}\text{Pb}$ populating the valence single-particle states of ^{209}Pb . In the inset a NFT($r+s$) diagram describing the process is shown. The energy of the outgoing proton reflects both the ground state Q -value of the reaction and the excitation energy of the final state (after Mottelson (1976b)).

Need of color

schematic

CHAPTER 1. INTRODUCTION

Correct all
other figures of
in the book
in this way

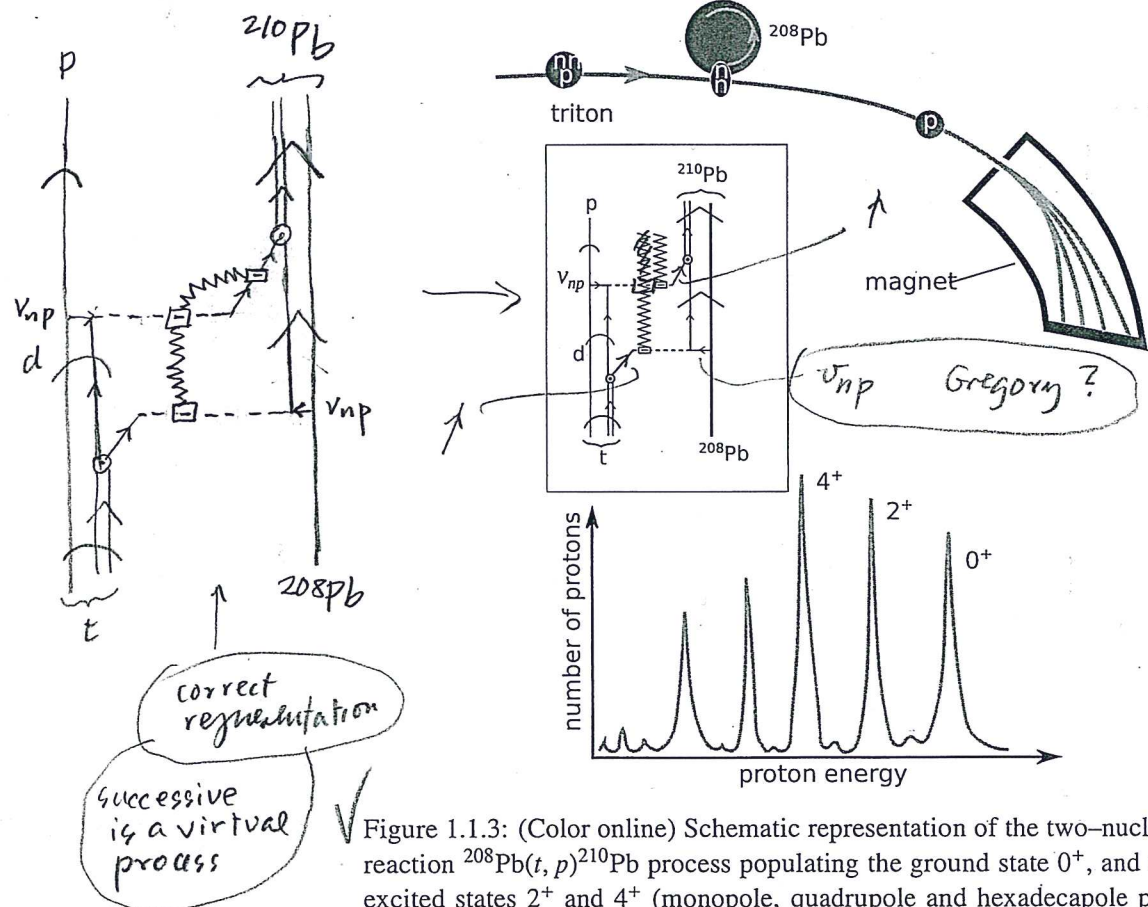
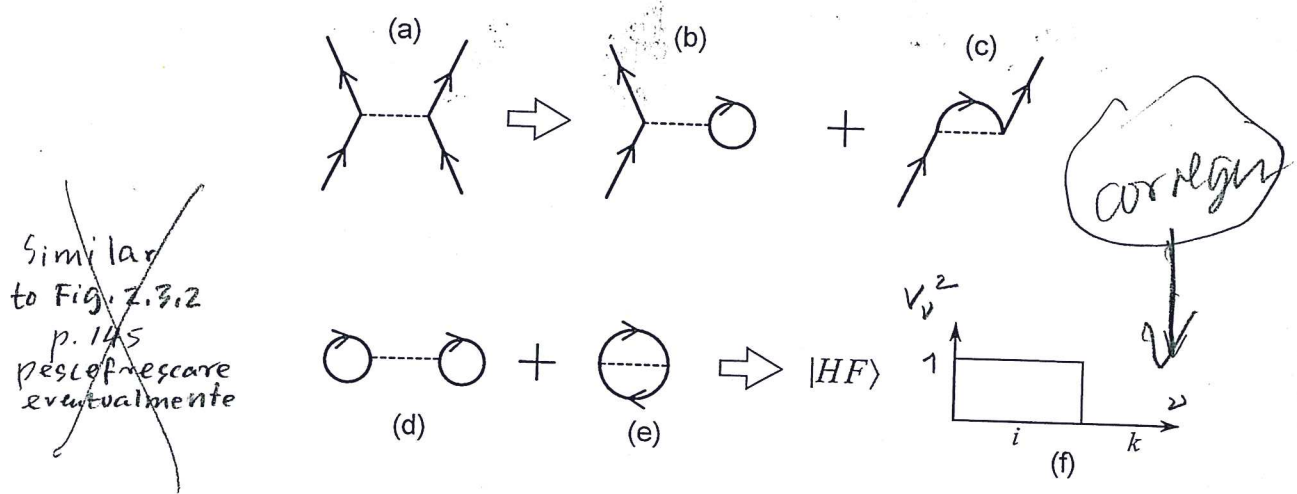


Figure 1.1.3: (Color online) Schematic representation of the two-nucleon transfer reaction $^{208}\text{Pb}(t, p)^{210}\text{Pb}$ process populating the ground state 0^+ , and two particle excited states 2^+ and 4^+ (monopole, quadrupole and hexadecapole pair addition modes of ^{208}Pb , i.e. multipole pariring vibrations (double arrowed line; App. 6.F), see Brink, D. and Broglia (2005) Sect. 5.3.1 p. 108, Broglia et al. (1974), Ragnars-son and Broglia (1976), Broglia, R. A. et al. (1971a), Broglia, R. A. et al. (1971b), Bès and Broglia (1971b), Bès and Broglia (1971a), Flynn et al. (1971), Bès et al. (1972), Broglia (1981), Bohr and Mottelson (1974), Flynn, E. R. et al. (1972), Bor-tignon et al. (1976); see also Kubo et al. (1970)). In the inset a NFT(r+s) diagram of the (successive) transfer process is displayed (after Mottelson (1976b)).

Need of color



$$\alpha_\nu |HF\rangle = 0; \quad \alpha_\nu = \begin{cases} a_k & (\epsilon_k > \epsilon_F) \\ b_i = (-1)^{\text{phase}} a_i^\dagger & (\epsilon_i \leq \epsilon_F) \end{cases}$$

✓ Figure 1.2.1: Schematic representation of the processes characterizing the Hartree-Fock ground state (single-particle vacuum), in terms of Feynman-NFT diagrams. (a) nucleon-nucleon interaction through the bare (instantaneous) NN -potential. (b) Hartree mean field contribution. (c) Fock mean field contribution. (d,e) ground state correlations (ZPF) associated with the Hartree and Fock processes. (f) There is, in HF (mean field) theory, a complete decoupling between occupied and empty states, labeled i and k respectively, and thus a sharp discontinuity at the Fermi energy of the occupation probability, from the value of 1 to 0. (g) This decoupling allows for the definition of two annihilation operators: $a_k(b_i)$ particle (hole) annihilation operators, implying the existence of hole (antiparticle) states ($b_i^\dagger |HF\rangle$) with quantum numbers time reversed to that of particle states, (for details see Brink, D. and Broglia (2005) App. A). In other words, the $|HF\rangle$ ground (vacuum) state is filled to the rim (ϵ_F) with N nucleons. The system with $(N-1)$ nucleons can, within the language of (Feynman's) field theory, be described in terms of the degrees of freedom of that of the missing nucleon (hole-, antiparticle state). Such a description is obviously considerably more economic than that corresponding to an anti-symmetric wavefunction with $(N-1)$ spatial and spin coordinates (\mathbf{r}_i, σ_i) . Within the above scenario, a stripping reaction $N(d, p)(N+1)$ can be viewed as the creation of a particle state ($a_k^\dagger |HF\rangle = |k\rangle$) and that of a pickup reaction $N(p, d)(N-1)$ as that of a hole state ($b_i^\dagger |HF\rangle \equiv |\tilde{i}\rangle$). *e.g.*

1.2. SUM RULES

21

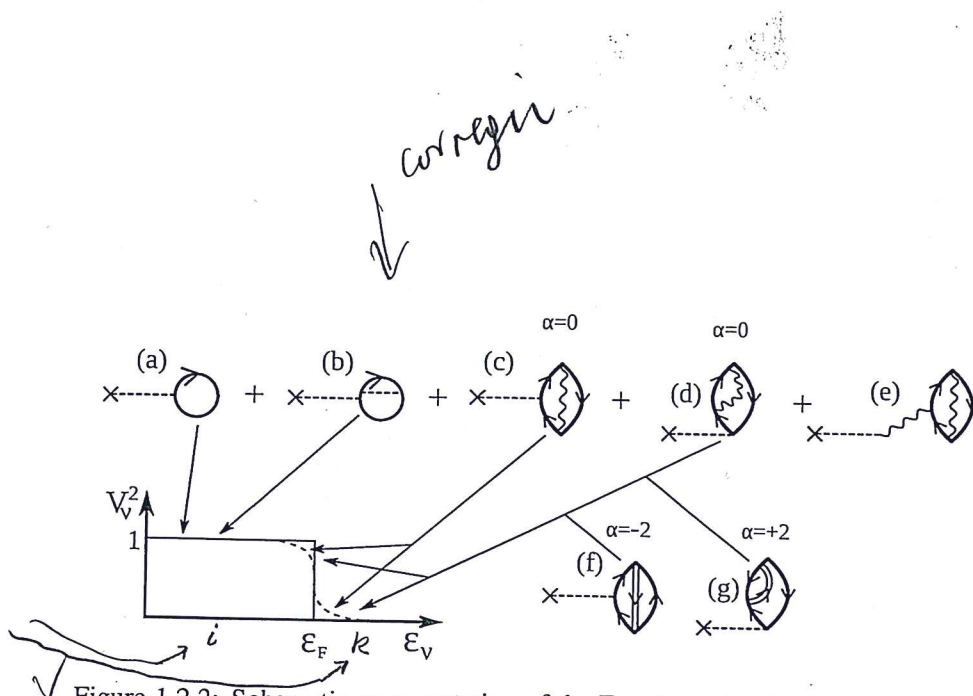


Figure 1.2.2: Schematic representation of the Fermi distribution. The sharp, continuous line drawn step function schematically represents the Hartree-Fock occupation numbers. The associated nuclear density measured with the help of an external field (cross attached to a dashed line) through processes of type (a) (Hartree: H) and (b) (Fock: F) is expected to display a diffusivity of the order of the strong force range. Zero Point Fluctuations (ZPF) associated with collective particle-hole state, i.e. processes with transfer quantum number $\beta = 0$ (Bohr (1964)) and shown in (c), (d) and (e), and with pairing vibrations, i.e. pair addition (graph (f)) and pair removal (graph (g)), smooth out the occupation numbers around the Fermi energy (dashed curve) and lead to a nuclear density of larger (dynamical) diffusivity than that associated with HF. One- and two-particle strengths which in this (mean field) approximation are found in a single A -mass system, are a result of ZPF ($\beta = 0, \pm 2$) distributed over a number of nuclei ($A, A \pm 2$) (see also App. 4.H, Fig. 4.H.1).

modes

$A \pm 1,$

$\pm 1,$

bold

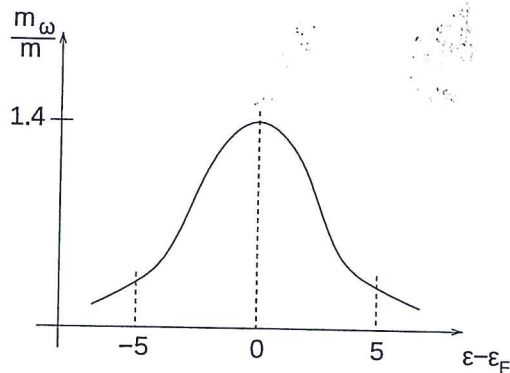
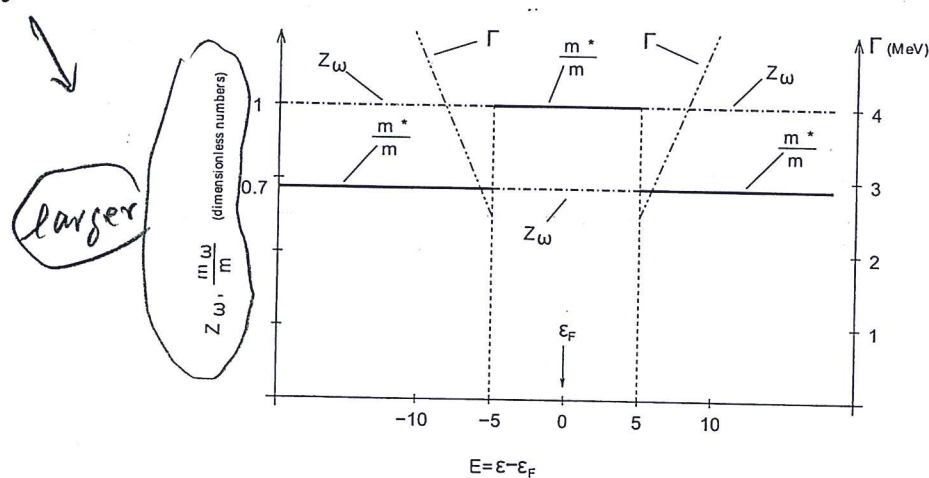


Figure 1.3.3: Schematic representation of the ω -mass as a function of the single-particle energy.



✓ Figure 1.3.4: Schematic representation of the behaviour of m_ω/m , $Z_\omega = (m_\omega/m)^{-1}$ and Γ as a function of $E = \epsilon - \epsilon_F$.

where \bar{V}^2 is the average value of $V_{\nu,\alpha'}^2$, while

$$n(\omega) = \sum_{\alpha'} \delta(\omega - E_{\alpha'}), \quad (1.3.22)$$

is the density of energy-conserving states α' . Eq.(1.3.21) is known as *Fermi Golden rule*.

Assuming the distribution of single-particle levels is symmetric with respect to the Fermi energy,

$$\Delta E(\omega) = \lim_{\Delta \rightarrow 0} \sum_{\alpha'} \frac{V_{\nu,\alpha'}^2 (\omega - E_{\alpha'})}{(\omega - E_{\alpha'})^2 + \left(\frac{\Delta}{2}\right)^2} = 0 \quad (1.3.23)$$

as there are equally many states pushing the state down than up (see Fig.1.3.5).

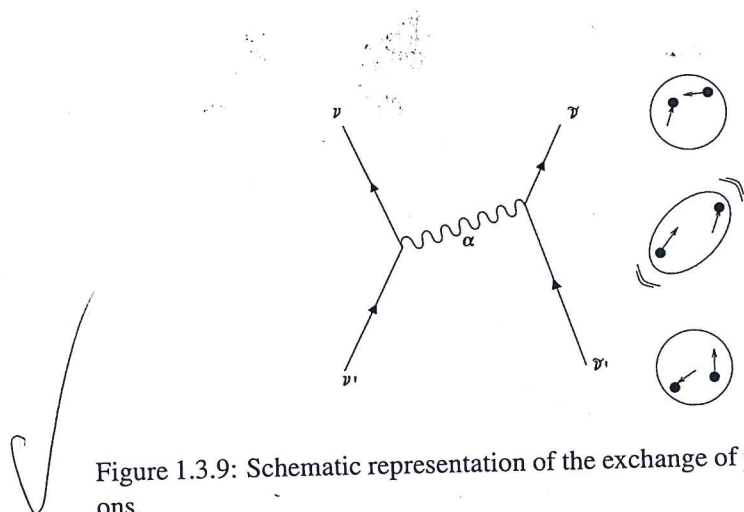


Figure 1.3.9: Schematic representation of the exchange of phonons between nucleons.

corregir

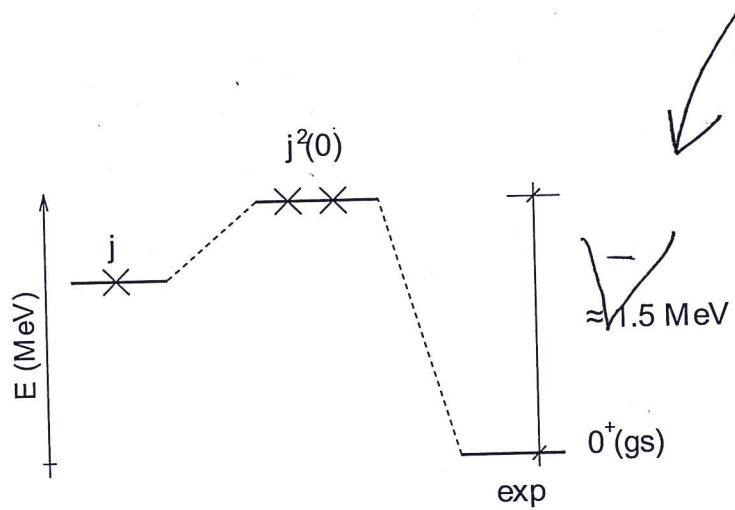
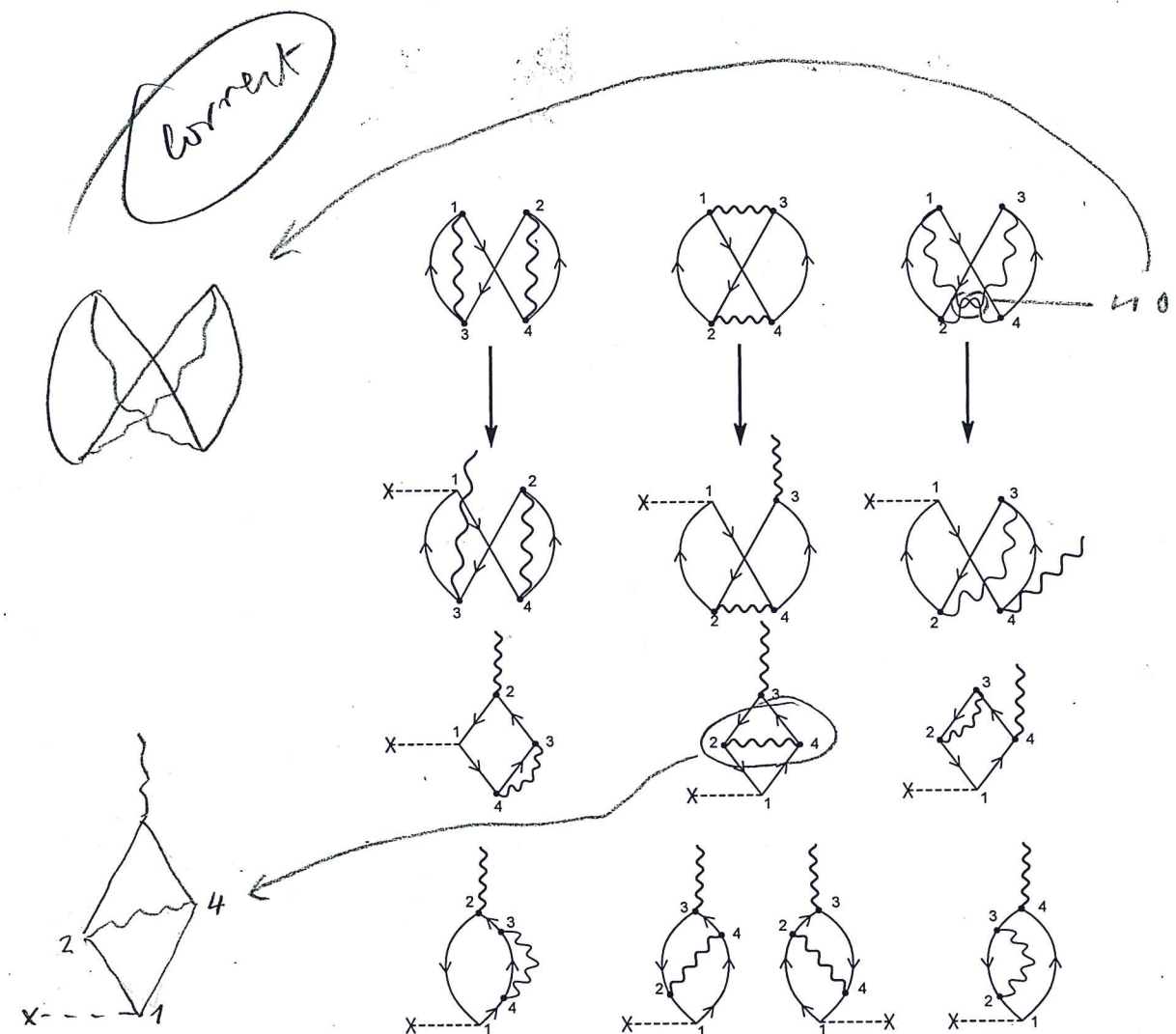


Figure 1.3.10: Schematic representation of the predictions of the independent particle model for one- and two-particles outside closed shell, in comparison with the experimental findings (e.g. for the case of ^{210}Pb , where $j = g_{9/2}$).

independent particle model



*no pueden
estar la
misma cultura
(retarded
int.)*

Figure 1.7.2: Some of the possible outcomes resulting from acting with a single-particle field, e.g. that associated with inelastic processes (represented by a horizontal dashed line starting with a \times), on the Pauli corrected ZPF oyster diagrams associated with collective ($p-h$) excitations of the nuclear vacuum (see Fig. 1.7.1). Within this context one returns to the question of renormalization mentioned in the text (see end of Sect. 1.1 and Sect. 1.4, see also Idini et al. (2015), Broglia et al. (2016), Barranco et al. (2017a); see also Sect. 6.5).

The possibility of using pairing vibrational modes as intermediate bosons contributing to the induced pairing interaction, not only in $^{\text{3}S_1}$ channels, but also in other multipole modes is discussed in App. 6.F.

In particular in connection 53 with the possible presence of "vortices" (pair addition mode of $J\pi = 1^-$ and $\beta = +2$ quantum numbers) in exotic, halo nuclei.

1.7. NUCLEAR FIELD THEORY FOR PEDESTRIANS

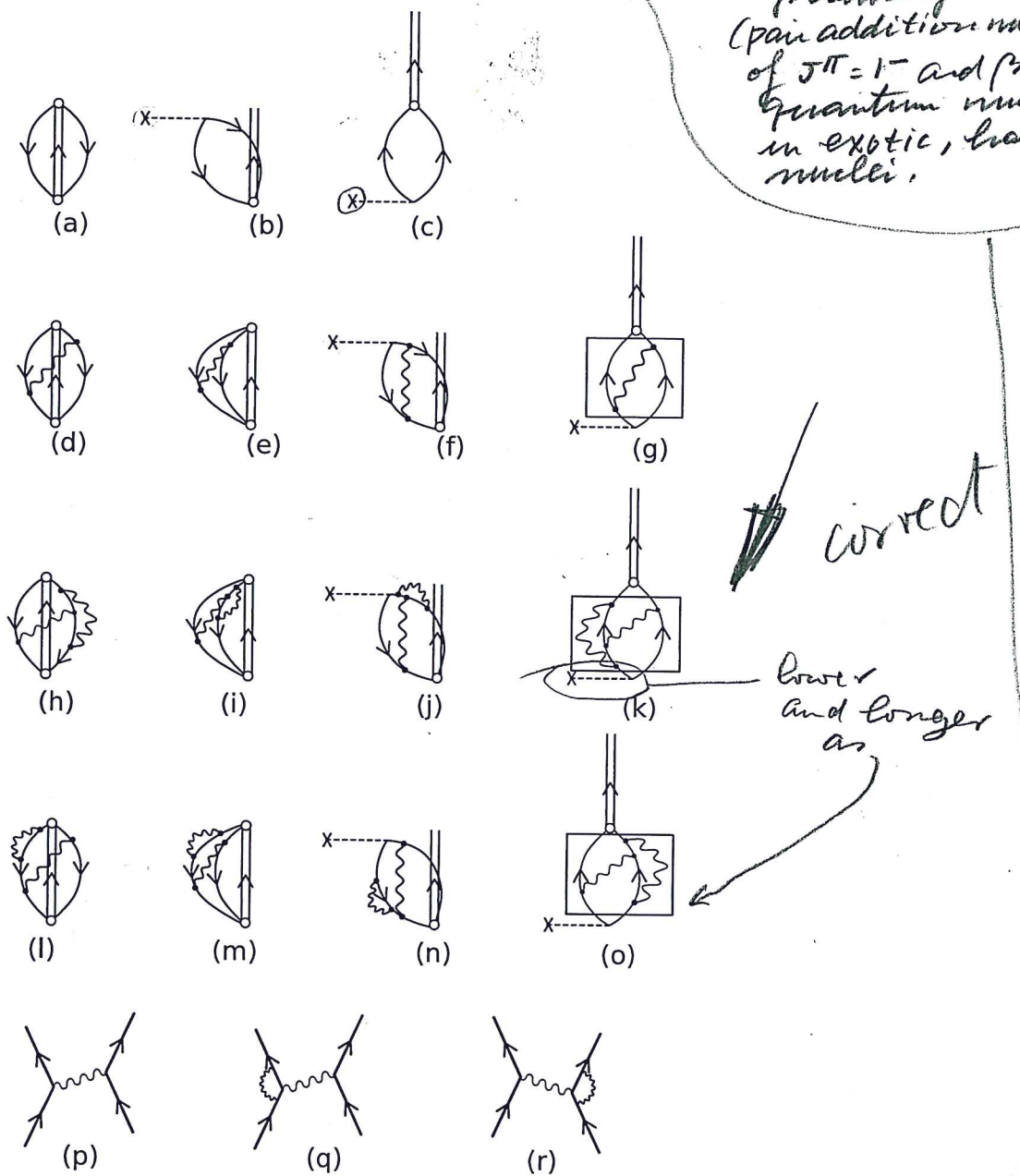
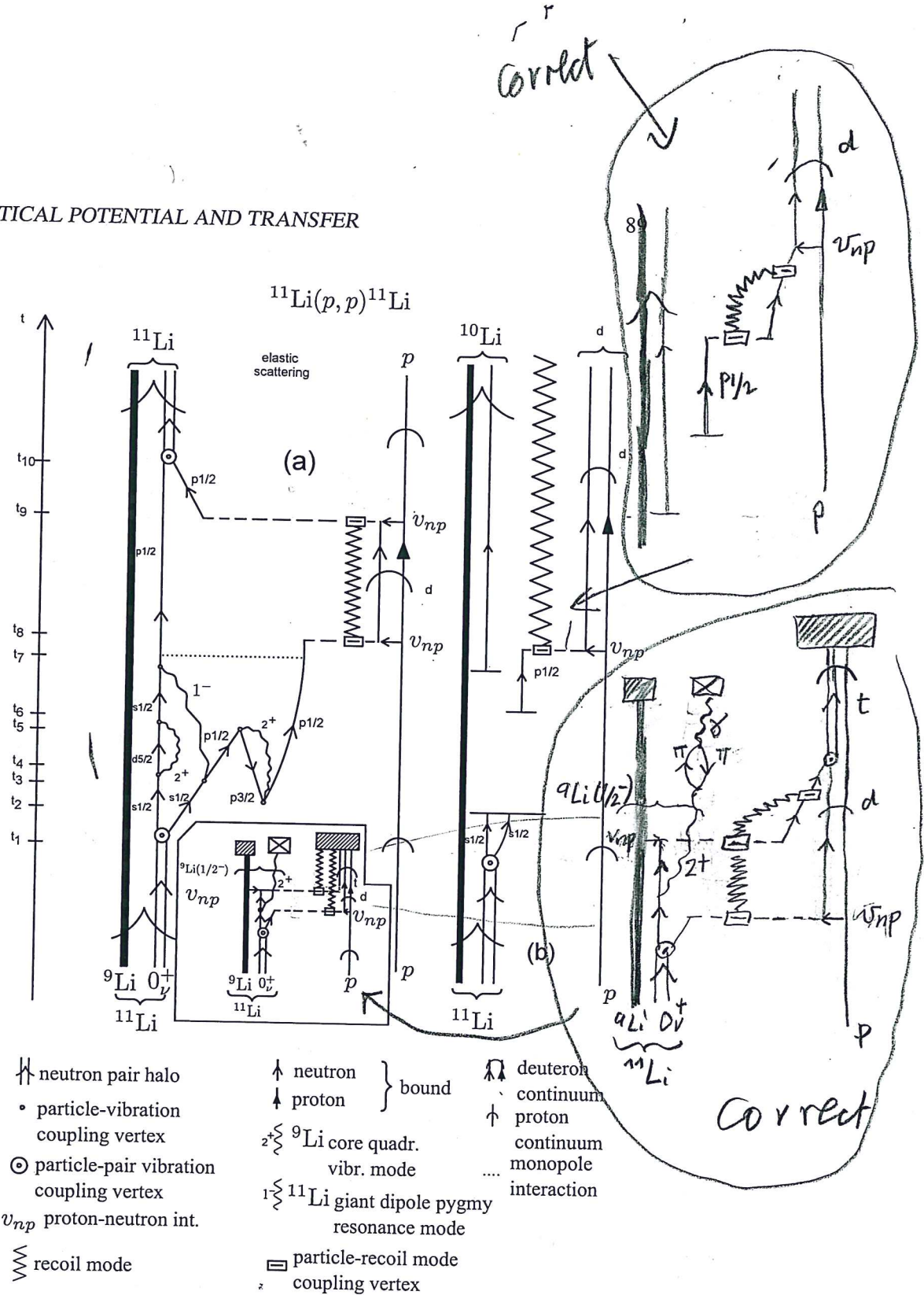


Figure 1.7.3: ZPF associated with the pair addition mode taking into account the interweaving of nucleons with density modes. The processes boxed in (g), (k) and (o), are associated with the induced pairing interaction (medium polarization effects; (p), (q), (r)) resulting from the exchange of density modes between nucleons moving in time reversal states, including also vertex corrections. The two-nucleon stripping and pickup external field is labeled by a dashed horizontal line which starts with a \times .

1.9. OPTICAL POTENTIAL AND TRANSFER



✓ Figure 1.9.2: (a) NFT-diagram describing one of the processes contributing to the elastic reaction $^{11}\text{Li}(p,p)^{11}\text{Li}$ as the system propagates in time (polarization contribution to the global (mean field) optical potential). In the inset, a schematic NFT diagram describing the process $^{11}\text{Li}(p,t)^{9}\text{Li}(1/2^-)$ is displayed. A crossed box represents a γ -detector, while hatched rectangles particle detectors. (b) Same as in (a) up to time t_8 (reason for which no details are repeated between t_2 and t_8). From there on the deuteron continues to propagate to the detector (together with the recoil mode). Likely, the neutron in ^{10}Li will break up before this event. Summing up, in the center of mass reference frame both p and ^{11}Li display asymptotic states in entrance as well as in exit channels in case (a), and only in the entrance channel in case (b), while in the exit channel only ^{10}Li ($^9\text{Li}+n$) and the deuteron do so.

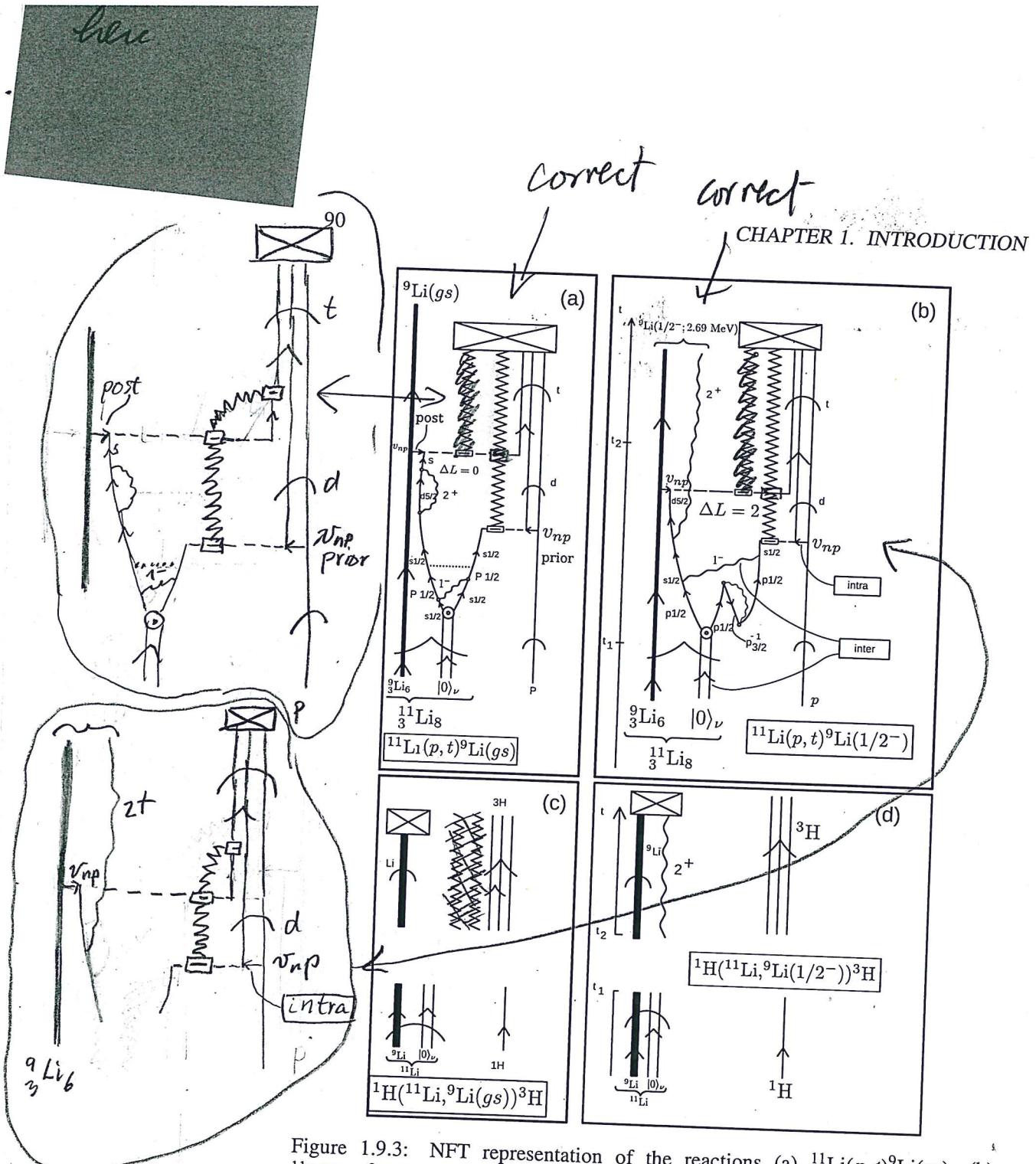


Figure 1.9.3: NFT representation of the reactions (a) $^{11}\text{Li}(p, t)^9\text{Li}(\text{gs})$, (b) $^{11}\text{Li}(p, t)^9\text{Li}(1/2^-)$, (c) $^1\text{H}(^{11}\text{Li}, ^9\text{Li}(\text{gs}))^3\text{H}$ and (d) $^1\text{H}(^{11}\text{Li}, ^9\text{Li}(1/2^-))^3\text{H}$. Time is assumed to run upwards. A single arrowed line represents a fermion (proton) (p) or neutron (n). A double arrowed line two correlated nucleons. In the present case two correlated (halo) neutrons (halo-neutron pair addition mode $|0\rangle_\nu$). A heavy arrowed line represents the core system $|^9\text{Li}(\text{gs})\rangle$. A standard pointed arrow refers to structure, while "round" arrows refer to reaction. A wavy line represents (particle-hole) collective vibrations, like the low-lying quadrupole mode of ^9Li , or the (more involved) dipole pygmy resonant state which, together with the bare pairing interaction (horizontal dotted line) binds the neutron halo Cooper pair to the core. A short horizontal arrow labels the proton-neutron interaction v_{np} responsible for the single-particle transfer processes, represented by an horizontal dashed line. A dashed open square indicates the particle-recoil coupling vertex. The jagged line represents the recoil normal mode resulting from the mismatch between the relative centre of mass coordinates associated with the mass partitions $^{11}\text{Li}+p$, $^{10}\text{Li}+d$ (virtual) and $^9\text{Li}+t$. The γ -detector and particle detectors are represented by a crossed rectangle. For further details see caption Fig. 1.9.2.

*correct
caption R*

*read
again
and correct
R*

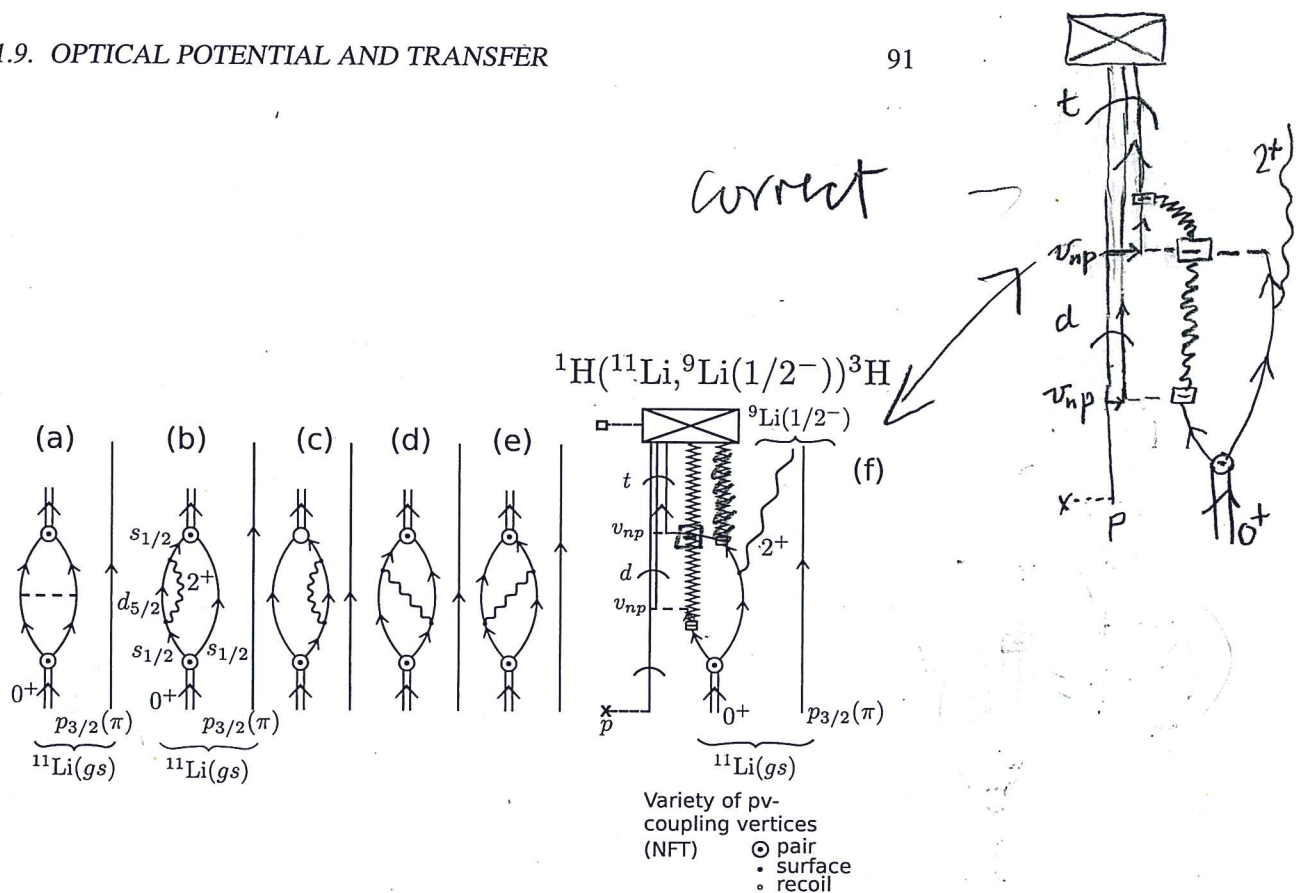


Figure 1.9.4: Lowest order, NFT diagrams associated with the processes contributing to the binding of the neutron halo Cooper pair (double arrowed line) of ^{11}Li to the core ^9Li through the exchange of the core quadrupole phonon (wavy line). Single arrowed lines describe the nucleon independent-particle motion of neutrons ($s_{1/2}$, $d_{5/2}$, etc.) as well as of protons ($p_{3/2}(\pi)$). (a) Bare interaction, four-point vertex (horizontal dashed line); (b, c) self energy, effective mass process dressing the $s_{1/2}(\nu)$ single-particle state; (d, e) vertex correction (induced interaction) renormalizing the vertex with which the pair addition mode couples to the fermion (dotted open circle); (f) NFT diagrams describing the inverse kinematics reaction $^1\text{H}(^{11}\text{Li}, ^9\text{Li}(1/2^-; 2.69 \text{ MeV}))^3\text{H}$ populating the first excited state of ^9Li . The jagged line represents the recoil mode carrying asymptotically to the detector the effect of the momentum mismatch associated with the transfer process (recoil). In this case of successive transfer, one for each transferred neutron ($^{11}\text{Li}(gs)+p \rightarrow ^{10}\text{Li}+d \rightarrow ^9\text{Li}(1/2^+) + t$). See also Sect. 2.6 as well as Sect. 6.1.

CHAPTER 1. INTRODUCTION

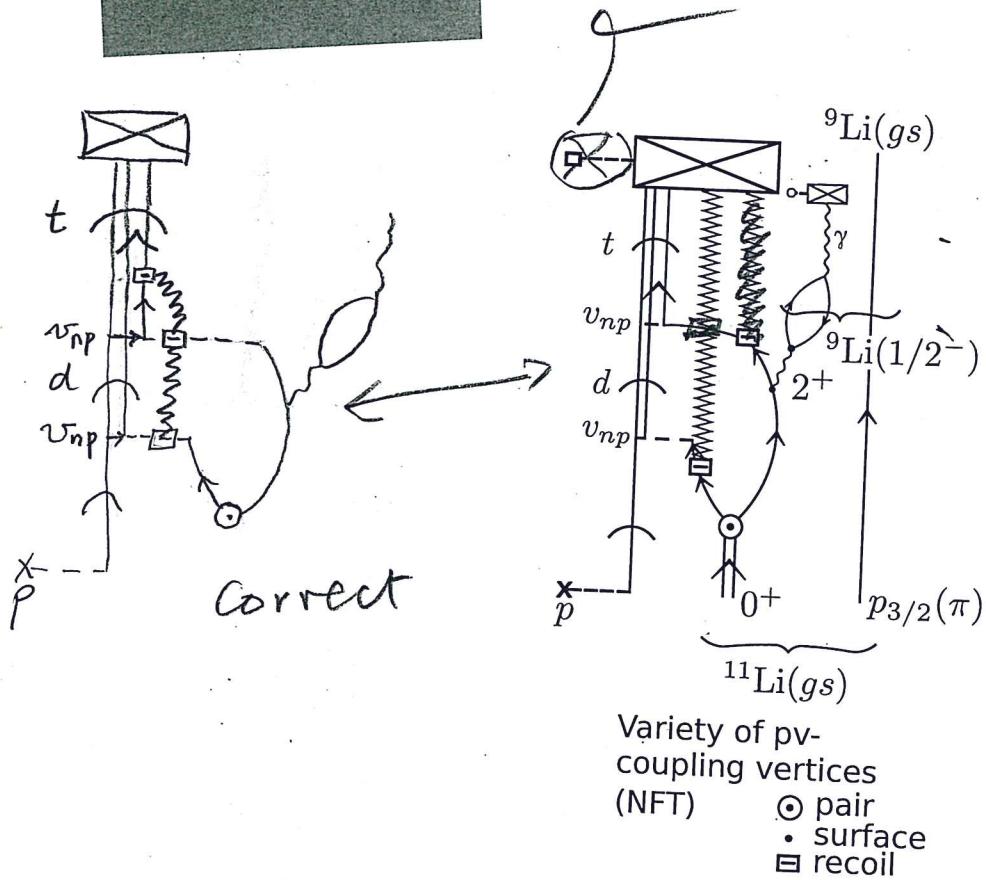


Figure 1.9.5: Gedanken γ -ray coincidence experiment $^1\text{H}(^{11}\text{Li}, ^9\text{Li})^3\text{H}$ and $^9\text{Li}(\text{gs}) + \gamma(E2; 2.69 \text{ MeV})$. In this case, the virtual quadrupole phonon associated with self-energy and vertex correction processes becomes real through the action of the (p, t) external field. Thus, it is not only that recoil modes are “measured” by detectors in connection with outgoing particles which have asymptotic wavefunctions, but also the quadrupole vibration, whose eventual γ -decay can be measured by the γ -detector.

*Correct
Capt P*

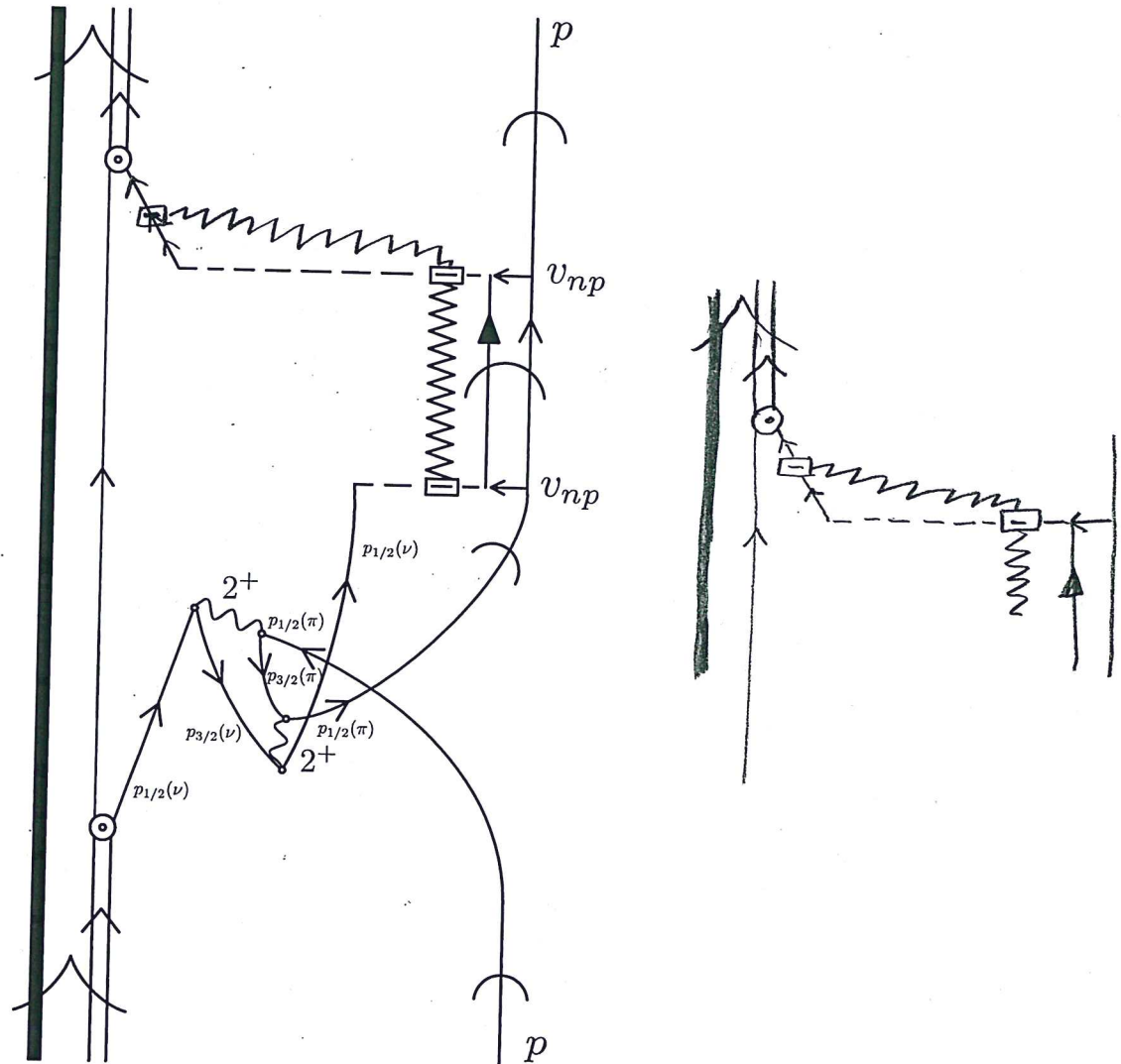
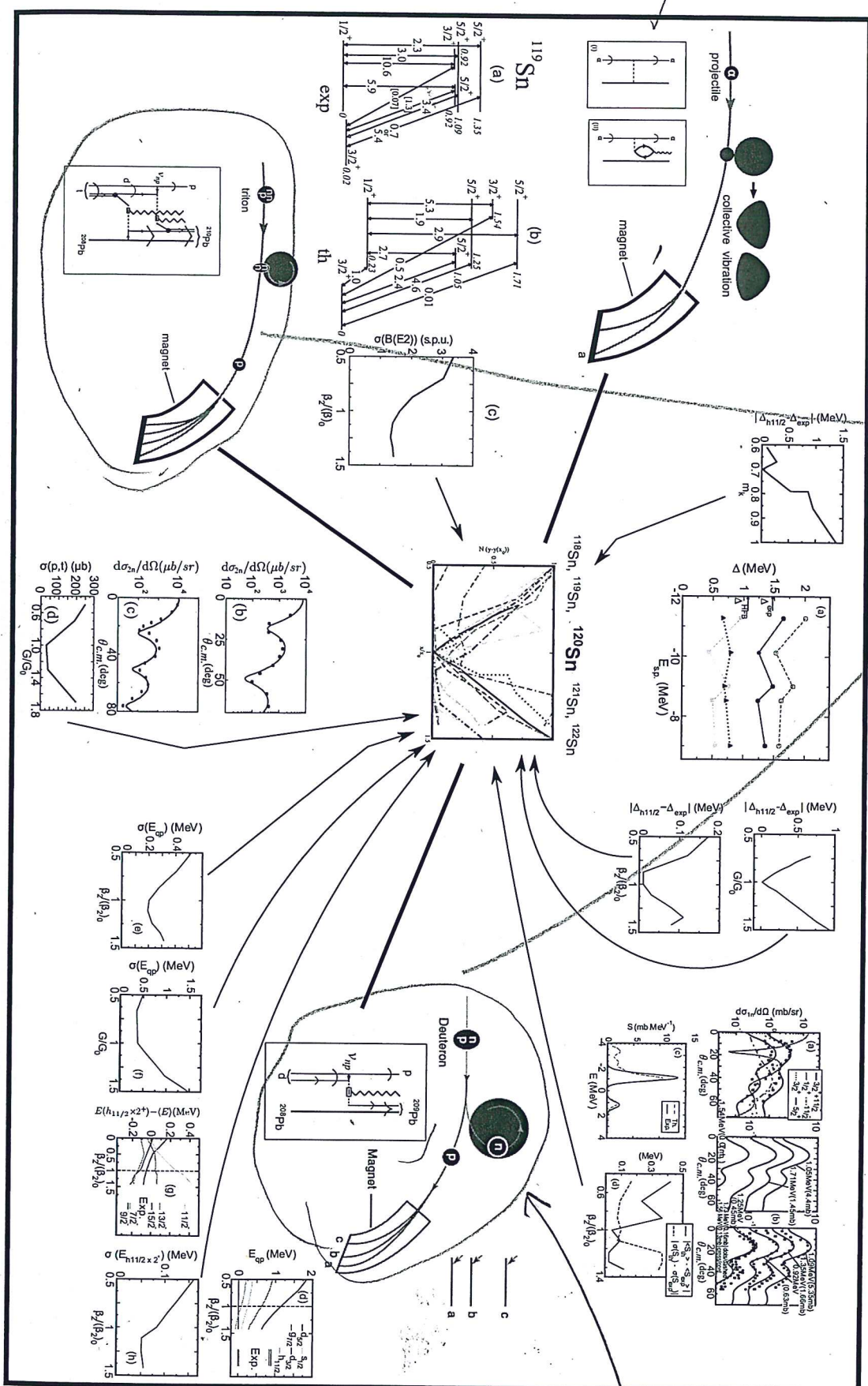


Figure 1.9.6: In keeping with standard direct reaction praxis, neither in Fig. 1.9.2 nor in 1.9.3 antisymmetrization is carried out between the impinging proton and the protons of ^{11}Li . Within the present discussion ($^{11}\text{Li}(p, p)^{11}\text{Li}$), an example of such processes corresponds to the exchange of a proton participating in the quadrupole vibration of the core, with the projectile, as shown in the figure. Such a process will not only be two orders higher in perturbation in the particle-vibration coupling vertex. It will be strongly reduced by the square of the overlap between a proton moving in the continuum, and a $p_{1/2}$ proton of the ^9Li core bound by about 10 MeV.

current logit

R

Figure 1.10.1: Characterization of ^{120}Sn .



regular
inelastic

one can write

$$\begin{aligned} \langle \Psi_\beta | V_\alpha - U_\alpha | \Psi_\alpha \rangle_{\mathbf{R}_{\alpha\beta}} &= \langle \Psi^b \Psi^B | (V_\alpha - U_\alpha) e^{i\sigma_{\alpha\beta}} | \Psi^a \Psi^A \rangle_{\mathbf{R}_{\alpha\beta}} e^{i\gamma_{\alpha\beta}} \\ &= \langle \phi^{B(A)}(S^B(n), r_{1A}), U(r_{1b}) e^{i\sigma_{\alpha\beta}} \phi^{a(b)}(S^a(n), r_{1b}) \rangle_{\mathbf{R}_{\alpha\beta}} e^{i\gamma_{\alpha\beta}}. \end{aligned} \quad (1.D.35)$$

To obtain the above relation, we have separated the difference between the phases δ_α and δ_β into a part $\gamma_{\alpha\beta}$ which only depends on time, and a phase $\sigma_{\alpha\beta}$ which also depends on the center-of-mass coordinate of the transferred particles. That is

$$\begin{aligned} \gamma_{\alpha\beta}(t) &= \int_0^t \left\{ U_\alpha(R_\alpha(t)) - \frac{1}{2} m_\alpha v_\alpha^2(t') - U_\beta(R_\beta(t')) + \frac{1}{2} m_\beta v_\beta^2(t') \right\} \\ &\quad + \mathbf{k}_{\alpha\beta}(t)(\mathbf{R}_\alpha - \mathbf{R}_\beta), \end{aligned} \quad (1.D.36)$$

where $\mathbf{k}_{\alpha\beta}$ is the average wave vector

$$\mathbf{k}_{\alpha\beta} = \frac{1}{2\hbar} (m_\alpha \mathbf{v}_\alpha(t) + m_\beta \mathbf{v}_\beta(t)). \quad (1.D.37)$$

Similarly

$$\sigma_{\alpha\beta} = \mathbf{k}_{\alpha\beta}(t) \cdot (\mathbf{r}_\beta - \mathbf{r}_\alpha). \quad (1.D.38)$$

The phase σ is characteristic for transfer processes since the dynamical variables \mathbf{r}_α and \mathbf{r}_β are identical for inelastic scattering. It arises from the change in the center-of-mass coordinate taking place when mass is transferred from one system to other. It gives rise to the recoil effect. Within the framework of DWBA it leads to a change of scaling of the DW (see also section elastic transfer). Summing up, the one-particle transfer amplitude reads

$$\begin{aligned} (a_\beta(t = +\infty))^{(1)} &= \int_{-\infty}^{\infty} \langle \phi^{B(A)}(S^B(n), \mathbf{r}_{1A}), U_{1b}(r_{1b}) e^{\sigma_{\alpha\beta}} \phi^{a(b)}(S^a(n), \mathbf{r}_{1b}) \rangle_{\mathbf{R}_{\alpha\beta}} \\ &\quad \times \exp \{i[(E_\beta - E_\alpha)t'/\hbar + \gamma_{\alpha\beta}]\} \end{aligned} \quad (1.D.39)$$

The phases $\delta_{\alpha\beta}$ play a similar role in the determination of transfer processes reaction amplitudes as δ_L does in connection with elastic scattering cross sections. In fact, $\delta_{\alpha\beta}$ determines the shift between incoming and outgoing waves and thus the interference process which is at the basis of the absolute value of the transfer differential cross section. In other words, the reaction part of the elastic and one-nucleon-transfer reaction cross section are embodied in δ_L and $\sigma_{\alpha\beta}$ respectively. The nuclear structure part is contained in the reduced mass μ and potential U in the case of elastic scattering, and in the single-particle wavefunctions, potential U_{1b} and Q -value phase in the transfer case. Within the diagrammatic representation of particle-transfer reaction theory, the recoil phase is represented by a jagged line. Similar to δ_L , $\sigma_{\alpha\beta}$ cannot be measured directly, but can in principle be inferred from the absolute differential cross section¹²⁸.

¹²⁸For more detail see Broglia and Winther (2004).

In other words, the jagged line does not display asymptotic behaviour, representing always a virtual process.

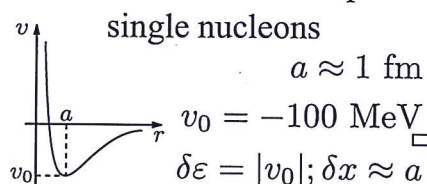
italic.

Classical localization and quantal ZPF

$$\delta x \delta k \geq 1 \quad \varepsilon = \frac{\hbar^2 k^2}{2M} \quad \delta k = \frac{\delta \varepsilon}{\hbar v_F} \quad (v_F/c \approx 0.3)$$

structure

Independent motion of



$$\delta x \delta k = \frac{a |v_0|}{\hbar v_F} \geq 1$$

Quantity parameter

$$q = \frac{\hbar v_F}{a |v_0|} \approx 0.6 \lesssim 1$$

delocalization

emergent property: generalized rigidity in
3D-space

how does a short range force lead to

single-nucleon mean free paths
larger than nuclear dimension?

$$2R \approx 20/k_F$$

answer: quantal fluctuations

reactions

single particle transfer, e.g. (p, d)

$$\frac{2R}{a} \approx 15$$

absolute cross section reflects the full nucleon probability amplitude distribution, and does not depend of the specific choice of v_{np}

Cooper pair transfer, e.g. (p, t)

$$\frac{\xi}{a} \approx 30 \text{ fm}$$

Successive and simultaneous transfer amplitude contributions to the absolute cross section carry ~~in a~~ ^{manner} equally efficiently information concerning pair correlations

Figure 2.4.2: Classical localization and zero point fluctuations, associated with independent-particle (normal density) and independent-pair motion (abnormal density).

quantal
fluctuations

phase correlations

OK

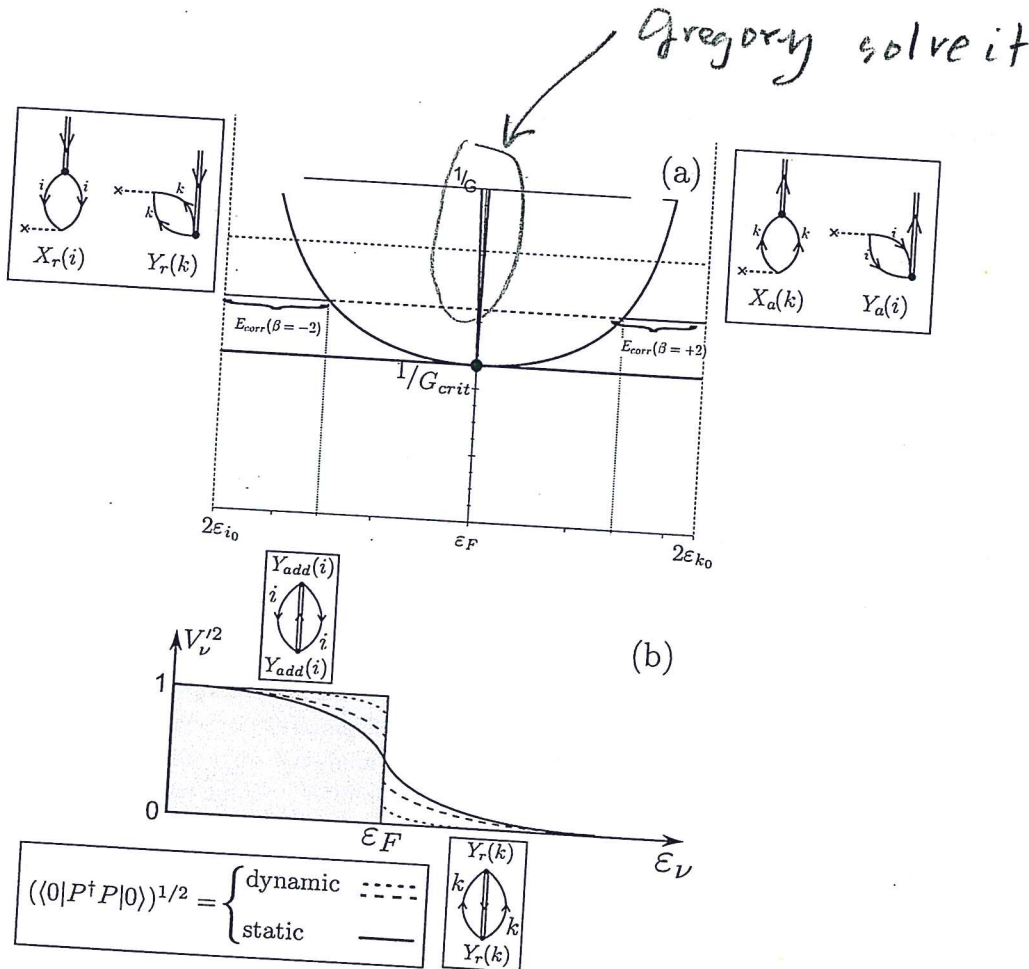


Figure 2.5.6: Schematic representation of the quantal phase transition taking place as a function of the pairing coupling constant in a (model) closed shell nucleus. (a) dispersion relation associated with the RPA diagonalization of the Hamiltonian $H = H_{sp} + H_p$ for the pair addition and pair removal modes. In the insets are shown the two-particle transfer processes exciting these modes, which testify to the fact that the associated zero point fluctuations (ZPF) which diverge at $G = G_{crit}$, blur the distinction between occupied and empty states typical of closed shell nuclei. (b) occupation number associated with the single-particle levels. For $G < G_{crit}$ there is a dynamical depopulation (population) of levels $i(k)$ below (above) the Fermi energy. For $G > G_{crit}$, the deformation of the Fermi surface becomes static, although with a non-vanishing dynamic component (cf. Fig. 2.1.2).

2.6. HALO PAIR ADDITION MODE AND PYGMY

173

correct

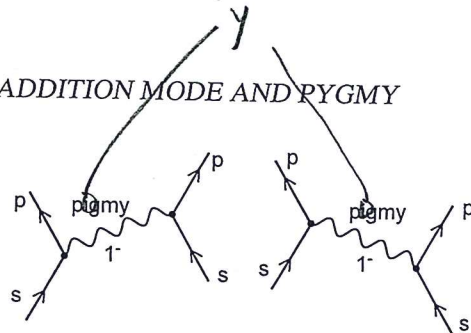


Figure 2.6.2: Diagrammatic representation of the exchange of a collective 1^- pygmy resonance between pairs of nucleons moving in the time-reversal configurations $s_{1/2}^2(0)$ and $p_{1/2}^2(0)$. It is of notice that both these configurations can act as initial states the figure showing only one of the two possibilities. Consequently, the energy denominator to be used in the simple estimate (2.6.11) is the average value $DEN = (DEN_1 + DEN_2)/2 = -\hbar\omega_{\text{pygmy}}$ where $DEN_1 = \Delta\epsilon - \hbar\omega_{\text{pygmy}}$ and $DEN_2 = -\Delta\epsilon - \hbar\omega_{\text{pygmy}}$, while $\Delta\epsilon = \epsilon_{s_{1/2}} - \epsilon_{p_{1/2}}$.

leading to $\Lambda \approx 0.6 \text{ MeV}$. The value of the induced interaction matrix elements is then given by (Fig. 2.6.2),

$$M_{\text{ind}} = \frac{2\Lambda^2}{DEN} \approx -\frac{2\Lambda^2}{\hbar\omega_{\text{pygmy}}} \approx -0.7 \text{ MeV}, \quad (2.6.11)$$

~~the factor of two resulting from the two time ordering contributions (see Fig. 2.6.2).~~ The resulting correlation energy is thus $E_{\text{corr}} = 2\epsilon_{s_{1/2}} - G' + M_{\text{ind}} \approx 0.4 - 0.1 - 0.7 \approx 0.4 \text{ MeV}$, in overall agreement with the experimental⁷⁹ findings (0.380 MeV). Of notice that in this estimate the (subcritical) effect of the screened bare pairing interaction has also been used (see Eq. (2.6.1))⁸⁰.

This schematic model has been implemented with microscopic detail⁸¹ within the framework of a field theoretical description of the interweaving of collective vibrations and single-particle motion, and is discussed in more detail within the context of single-particle (Chapter 4) and two-particle (Chapter 6) transfer processes. Here we provide a summary of the theoretical findings.

In Fig. 2.6.3 (I), the single-particle neutron resonances in ${}^{10}\text{Li}$ are given⁸². The position of the levels $s_{1/2}$ and $p_{1/2}$ determined making use of mean-field theory is shown (hatched area and thin horizontal line, respectively). The coupling of a single-neutron (upward pointing arrowed line) to a vibration (wavy line) calculated making use of NFT Feynman diagrams (schematically depicted also in terms of either solid dots (neutron) or open circles (neutron hole) moving in a single-particle level around or in the ${}^9\text{Li}$ core (hatched area)), leads to conspicuous shifts in the energy centroid of the $s_{1/2}$ and $p_{1/2}$ resonances (shown by thick horizontal lines)

⁷⁹C. Bachelet et al. (2008), M. Smith et al. (2008).

⁸⁰That new physics, namely a novel mechanism to (dynamically) violate gauge invariance, finds a scenario of a barely bound Cooper pair at the drip line (half life 8.75 ms) to express itself seems to confirm a recurrent expectation. That truly new complex phenomena appear at the border between rigid order and randomness (see de Gennes (1994)).

⁸¹cf. Barranco, F. et al. (2001).

⁸²See however Cavallaro et al. (2017).

$$E_{\text{corr}} = 2\epsilon_{s_{1/2}} - (G)_{\text{scr}} + M_{\text{ind}} = (0.4 - 0.1 - 0.6) \text{ MeV} \approx -0.3 \text{ MeV}$$

0.5
0.2

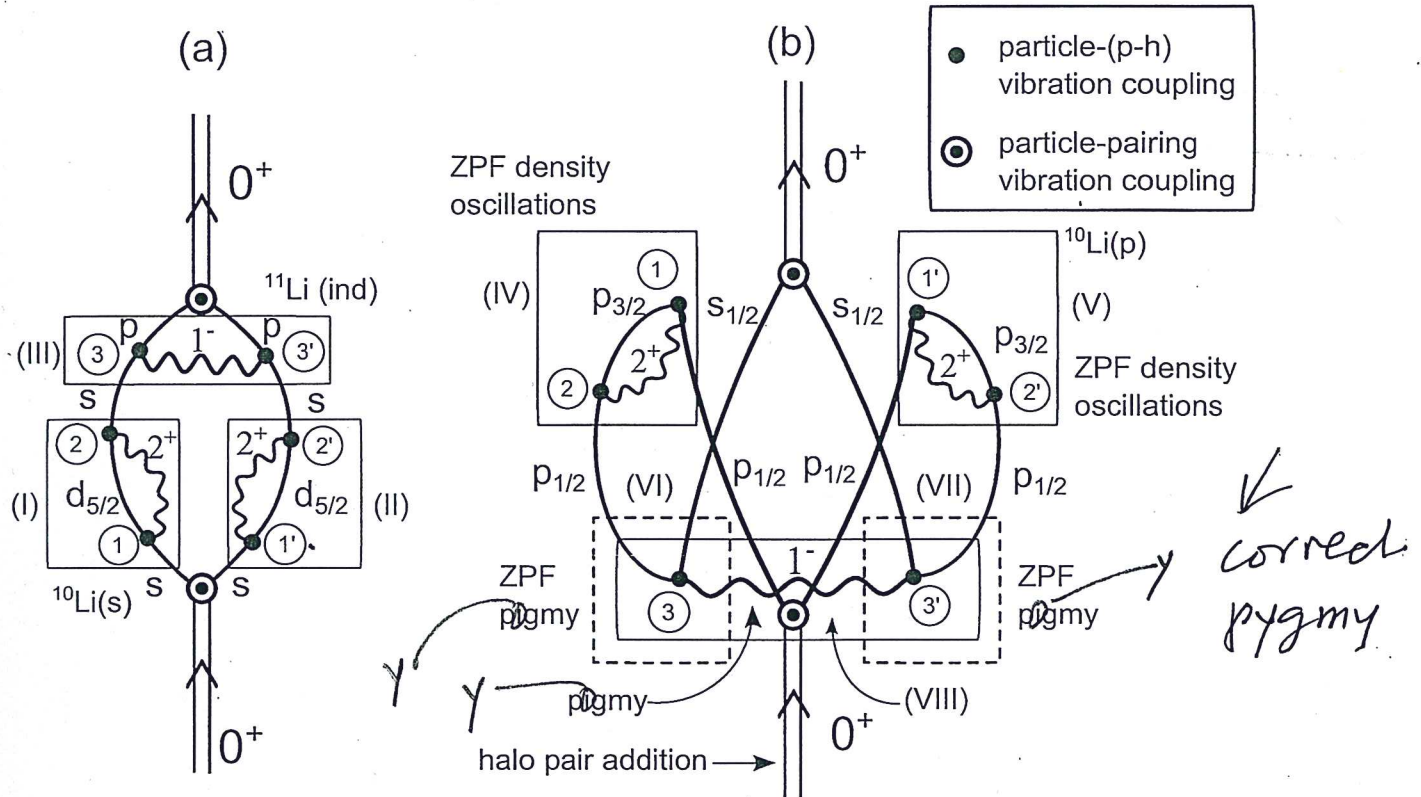


Figure 2.A.1: NFT Feynman diagrams describing the binding of the halo Cooper pair through pygmy. That is, producing the symbiotic mode involving the pair addition mode and the GDPR. The single-particle states $s_{1/2}$ and $p_{1/2}$ are labeled in (a) s and p for simplicity. The different particle-vibration coupling vertices (either with the quadrupole (2^+) or with the pygmy (1^-) modes drawn as solid wavy lines) are denoted by a solid dot, and numbered in increasing sequence so as to show that diagram (b) emerges from (a) through time ordering. The motion of the neutrons are drawn in terms of continuous solid curves. In keeping with the fact that the occupation of the single-particle states is neither 1 nor 0 (cf. Eqs. (6.1.1)–(6.1.3)), these states are treated as quasiparticle states. Thus no arrow is drawn on them. Diagram (a) emphasizes the self-energy renormalization of the state $s_{1/2}$ lying in the continuum and which through its clothing with the quadrupole mode is brought down becoming a virtual ($\epsilon_{s_{1/2}} = 0.2$ MeV) state (see (I) and (II)), while (III) contributes to the induced pairing interaction through pygmy (see also Fig. 2.6.2). The “eagle” diagram (b) contains (cf. (IV) and (V)) Pauli corrections which push the bound state $p_{1/2}$ into a resonant state in the continuum ($\epsilon_{p_{1/2}} = 0.5$ MeV). In other words, processes (I), (II), (III), (IV) and (V) are at the basis of parity inversion, and of the appearance of the new magic number $N = 6$. Processes (VI) and (VII) are associated with the pygmy ZPF, while (VIII) contributes to the induced pairing interaction through pygmy (van der Waals-like process).